Systematic Investigation of Premixed Methane Impinging Flames

Jin Fu*[,1], C.W. Leung[1], Zuohua Huang[2], C.S.Cheung[1], Yang Zhang[3]

[1]Department of Mechanical Engineering, Hong Kong Polytechnic University, Hung Hom, Kowloon, Hong Kong
[2]State Key Laboratory of Multiphase Flow in Power Engineering, Xian Jiaotong University, Xian, China
[3]Combustion and Flow Diagnostics Laboratory, Department of Mechanical Engineering,
Sir Frederick Mappin Building, University of Sheffield, Sheffield S1 3JD, UK

Abstract

Turbulent impinging flame dynamics were investigated using methane/air Busen flames with the methods of OH-PLIF, high-speed color imaging, thermal imaging and acoustic recording as well as DFCD and FFT post process. The main aim of this paper is to investigate turbulent flame pattern variations and their correlation with the temperature distribution across an impinging plate. Results showed that, the alteration in the plate-to-nozzle distance results in the discernible variations in the radial temperature distribution. Meanwhile, distinct audible flame noise varied with the change of impinging flame structures.

Introduction

Flame impingement is widely found in many industrial and domestic combustion systems to facilitate the confinement of energy for an effective generation of energy for motion and/or heat transfer. Thus, the profiling of the different operating configurations to examine the optimum interaction between flame and impinging plate for a given process is an important research topic.Commonly, this is done to get a better understanding of the relationship between the target surface temperature with the reactant flow and geometry parameters such as plate-to-nozzle distance, equivalence ratio, flame burning modes and ignition location. Fuel composition variability is perhaps the most widely examined factor in impinging flame studies. For example the effect of thermal radiation on heat transfer process of the oxy-natural gas impinging flames[1-3], interacting methane/air flame jets at stoichiometric condition [4], and concurrent simulation on methane/air impinging combustion process [5] were studied. Investigations on other fuels were also carried out in recent years to examine the emissions and heat transfer of impinging flame characteristics of hydrogen and LPG mixed gases [6-9]. In diffusion flame investigations, Dong et al [10-12] conducted series of work on the impinging flame structure and the associated heat transfer processes. Meanwhile, complementary modeling studies were also conducted [13, 14] and laser-based diagnostic techniques were also used in the study of the impinging flame. Boxx et al [15] used the OH-PLIF technique to identify and track both the spatial position and the shape of the flame-front, while the stereoscopic PIV was used to measure three-component planar velocity over the same region. Similarly, Yu et al [16] used the PLIF to study the flame structures. Investigation on burning and heat transfer processes of domestic natural-gas stoves were also attempted [17], [18]. Some other works and review articles on turbulent impinging flames and flame stability were also presented [19-26].

Few researches, however, reported on turbulent flames and the flame induced acoustic effect are limited. Thus, in this study, turbulent flames and its acoustic characteristics were studied using several equipment. Acoustic data and digital flame images were acquired using a microphone and a high-speed color camera along with the measurement of OH radical distribution by OH-PLIF to analyze the spatial flame dynamic variation and its effect on temperature distribution.

Experimental setup

A schematic illustration of the experimental setup is shown in Fig.1. A Bunsen burner with an internal nozzle diameter of 4.5 mm was used and placed under a metallic vertical traverse platform which is designed to support an oxidized steel impinging plate (300 mm in diameter, 10 mm in thickness) orthogonal to the reactant flow direction. Gaseous methane (CH4) and air were delivered from their individual cylinders and controlled by dedicated electronic flow controller through the LabView signal interface. The ratio of flame-to-nozzle distance (h) and nozzle diameter (d) varies from 6.66 to 15.5. Turbulent flames were studied at XCH4 = 0.33 (CH4 = 2 L/min, Air = 4 L/min, Reynolds number = 2540) under which condition that flames structures change with the impinging distance while not too big that may blow off.

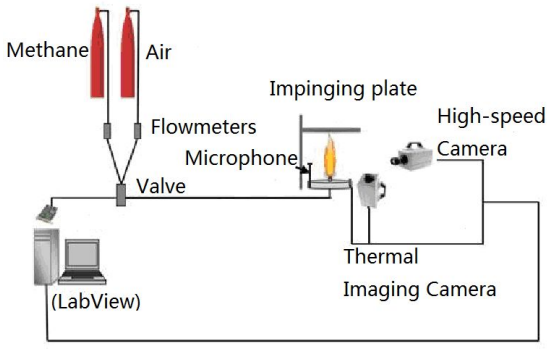

Fig.1 Schematic layout of experimental setup.

*Corresponding author: jin.fu@polyu.edu.hk

Video recordings of the dynamic plate temperature variations were captured using a FLIR SC3000 thermal-imaging camera operating at 7 frames per second (fps). The corresponding high-speed flame color images were extracted from the video taken by a Photron SA4 high-speed camera operating at 500 fps. The raw image data were post-processed by DFCD (Digital Flame Color Discrimination) to separate different flame color entities for the localized FFT (Fast Fourier Transformation) processing to extract the flame oscillation frequency spectrum[27, 28]. Flame OH radical distributions were captured by OH-PLIF and details of the equipment has been reported in the literature[29]. Acoustic data were captured using a PCB 377C10 precision condenser microphone (frequency range of 4 to 70k Hz) sampled through the LabView interface at a rate of 5000Hz.

In this study, the distance between the plate and thermal imaging camera was fixed at 0.9 m. The plate has an estimated emissivity of 0.79, and its initial temperature is controlled at 25^{o}C before impingement heating. In each case, flame impingement was maintained for 10 minutes, which was then extinguished temporally to record the thermal profiles of the steel plate. The radial temperature distribution along the radius of the plate was measured from the stagnation point at the center towards the plate edge. One second of high-speed flame images was recorded prior to the flame extinguish for the start of thermal image recording. Acoustic noise was collected at the same 3 centimeters away from the nozzle. During the flame measurements, both flame high speed images and acoustic data were collected simultaneously while the OH-PLIF images were captured under the identical conditions.

Results and discussion

3.1 Turbulent flame shape variations

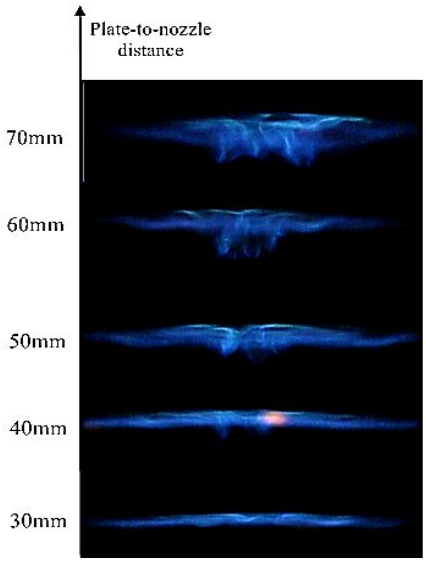

Fig.2 Flame structures under different impinging distance.

Figure 2 shows the impinging flames under varied flame-to-nozzle distance. Flame structure becomes more wrinkled and distorted with a widening of the turbulent flame area with increase of flame-to-nozzle distance. Study on different impinging burning modes [14] showed the appearance of ring and disc flame structure as a result of variation of geometry-induced local reactant mixture. An increase in h/D distance enhances the shear mixing of flow reactants with the surrounding atmosphere. As a result, the reactant composition in the cases in Fig. 2 is expected to be significantly fuel-leaner than that in the upstream region around the nozzle exit. Combustion front occurs along the line of most reactive mixture fraction [30], and this results in the change of flame mode and structure with the increase of h/D as the reaction expands to new reaction front in response to the geometric-induced composition variation. This phenomenon can be explained by the flame turbulence effect.

Figure 3 shows the instantaneous OH-PLIF distribution of turbulent impinging flames at h=65 mm and 55 mm respectively. A similar insight to that observed from the color images is presented. As h/D increases, flame becomes more turbulent and there are more vortexes under the same inlet flow rate. At 55 mm, flame detaches from the nozzle and becomes a ring shape flame [31] with little vortex structure. When nozzle-to-plate distance increases to 65 mm, the vortex in the flame become more obviously and disc flame shape with vortex confinement to the region around the stagnation point is presented. The OH-PLIF image indicate the OH radical distribution of flames. If more reddish color shown in the flame, then it means more OH radicals exist in the area, which also means the combustion is more intensive in the area [29].

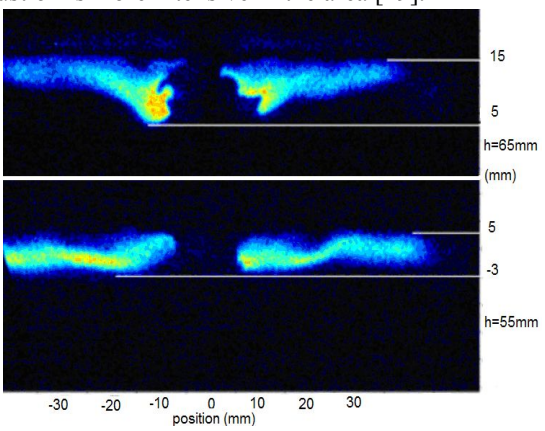

Fig.3 Flame OH-PLIF images at h=65mm and h= 55mm.

When flame-to-nozzle distance increases from 55 mm to 65 mm, the flame vortex thickness increases from 8 mm to 11 mm. Therefore, the geometric-induced combustion turbulence contributing to different heat transfer profiles and may have a significant effect on material and geometric design in the confined engine environment.

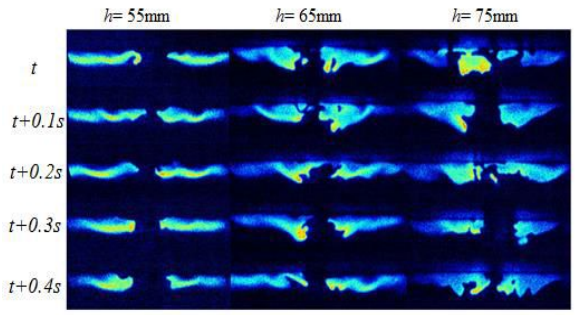

Fig.4 Flame structure variation along impinging distance from 55mm to 75mm within 0.5 second

In order to get a comparison of continuous flame structure variations along different impinging distance (h), OH-PLIF images were taken at different conditions. Fig.4 shows the overall flame structure changes in three impinging height with a interval of 10mm from 55mm to 75mm, in continuous 0.5 seconds. At 55mm, the flame structures didn't change much within 0.5 seconds and the flame looks quite flat with a little vortex in the center area. However, as the impinging distance get higher, the flame turbulence effect tends to perform stronger and the center of flames begin to get thicker because of the flame vortex. When the distance reaches 75mm, the flame vortex become quite strong and flame structure varies differently within 0.5 seconds with flame vortex not only existing in the center of the flames but .

3.2 Heat transfer and temperature distribution of impinged plate

As the flame structure variations has been studied, we started to wonder if there any temperature distribution differences induced by the flame structures. Therefore, temperature measurement along the radial direction of the plate with flame turbulence as shown in Fig.5.

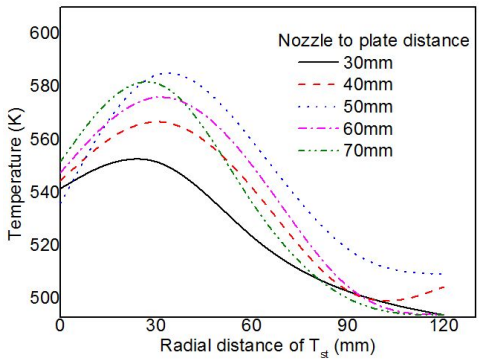

Fig. 5 Plate temperature distributions according to different flame shapes depicted in Fig. 2.

From the figure, we can see that from h=30 to 60 mm, with the increase of plate height, the overall temperature along the plate surface get higher and the position of peak temperature shifts towards the plate edge with the increase of h. However, at h=70 mm, the turbulence becomes prevalent and the peak temperature position reverses to move inward towards the plate center with a reduction in the observed peak temperature. This phenomenon can be explained by the flame vortex variations. At the first place, when the flame vortex get stronger, flame structure changes from flat flame to more turbulent flame and the peak temperature point tends to move outwardly from the near center position. However, when impinging height increases too much, flame might get even more leaner and the flame temperature might drop and because of the more turbulent flame structures (shown in Fig. 4), the peak temperature point might move inwardly.

3.3 Combustion noise studies under different impinging distance

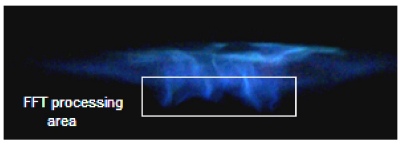

Fig.6 FFT processing area A extracting from original picture.

Beside variations of flame structure and plate temperature, the combustion noise changes were also discovered during experiments. Therefore, microphone controlled by LabView interface was used to measure the acoustic data of turbulent flames. Figure 6 shows the flame oscillation characteristics with the localized FFT processing of the flame reaction center near the stagnation point, and the comparison between the acoustic and image-derived FFT oscillation profiles are given in Fig. 7.

A peak around 45Hz is clearly shown in both the acoustic and imaging data after the FFT processing. The peak of power spectrum of acoustic data at 45Hz well coincides with that observed from the flame oscillation. The flame turbulence leads to both audible flame burning noise and temperature enhancement induced by turbulence with 45Hz oscillatory dynamics.

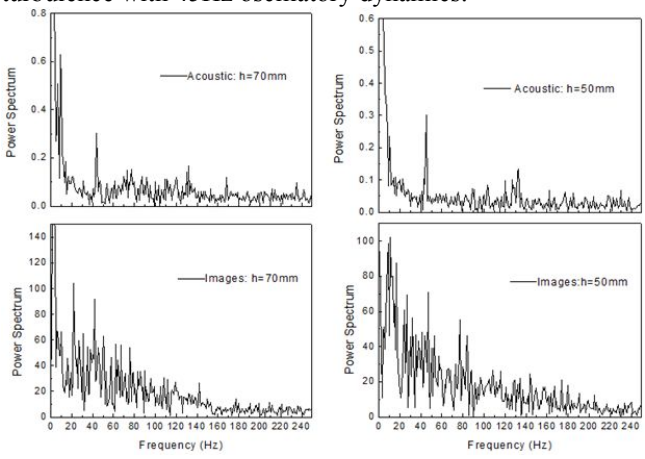

Fig.7 Acoustic and images frequency data results shown in spectrum after FFT.

In order to rule out the possibility of the side part flame induced combustion noise. Same study about the

side part of the turbulent flames was also conducted in Fig. 8 and Fig. 9. At this time, the side part of turbulent flames was the target to investigate.

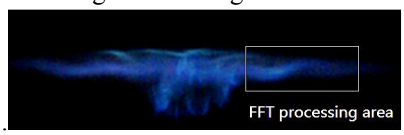

Fig.8 FFT processing area B extracting from original picture

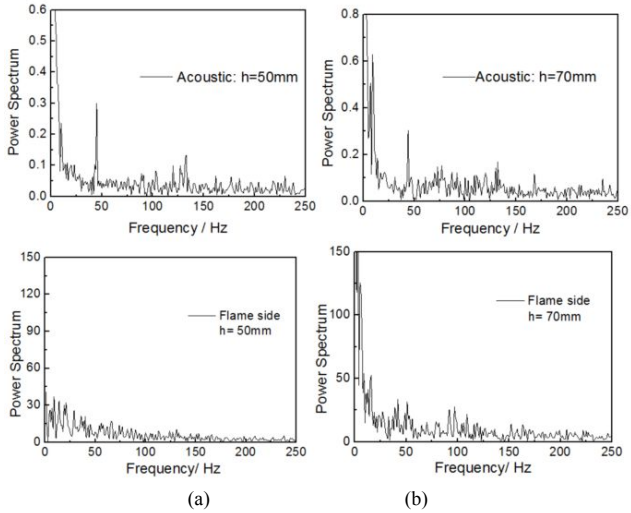

Fig.9 Acoustic and side flame frequency data results shown in spectrum after FFT.

From the frequency spectrum shown in Fig. 9, we cannot find any relationship between the side flame structure variation and the combustion noise. Therefore, we can conclude that the inner part of turbulent flame structure variations have influence on the combustion noise changes along the impinging height.

According to the result in Fig. 7, power spectrum which represents the intensity of frequency was measured at 45Hz. The results show a tremendous growth of signal intensity with increased nozzle-to-plate distance as shown in Fig.10.

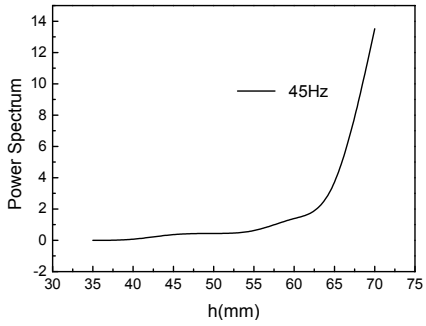

Fig.10 Intensity of 45Hz frequency varied with nozzle-to-plate distance.

Plate-to-nozzle distance improves the turbulence of flame especially at the downside of impinging flames. The intensity of combustion noise variation shows that, the noise increased dramatically after h=63 mm, which is correlated to the flame structure change along the impinging height.

Conclusions

Results of this experiment showed a great consistence between acoustic signal and images after fast Fourier transform (FFT) in turbulent impinging flames and same trend between image signal power spectrum and flame turbulence. Laminar partial premixed flames shows an interesting trend on temperature distributions on the target plate. Those results are very useful in the improvement of the domestic burner designs.

Main conclusions are summarized as follows:

1. It was found that impinging distance changes the plate temperature distribution.

2. Plate-to-nozzle distance has a significant effect on flame shapes. Plate-to-nozzle distance also affects the intensity of central flame turbulence.

3. Acoustic samples and imaging samples of turbulent flames show the same peak of frequency after the FFT processing and this reveals that combustion noise is linked to flame vortex shedding.

Acknowledgments

This work is supported by the Financial Assistance from GRF of HKSAR (Project No. B-Q39F), National Natural Science Foundation of China (Grant No. 51136005, 51121092) and the National Basic Research Program (2013CB228406).

References

[1] C. E. Baukal; B. Gebhart, Experimental thermal and fluid science 15 (4) (1997) 323-335
[2] C. E. Baukal; B. Gebhart, International Journal of Heat and Mass Transfer 40 (11) (1997) 2539-2547
[3] C. Baukal; B. Gebhart, Experimental thermal and fluid science 16 (3) (1998) 247-259
[4] S. Chander; A. Ray, International journal of heat and mass transfer 50 (3) (2007) 640-653
[5] S. Chander; A. Ray, International Journal of Heat and Mass Transfer 51 (13) (2008) 3595-3607
[6] H. Li; H. Zhen; C. Leung; C. Cheung, International Journal of Heat and Mass Transfer 53 (19) (2010) 4176-4184
[7] H. Li; H. Zhen; C. Leung; C. Cheung, International Journal of Heat and Mass Transfer 54 (1) (2011) 625-635
[8] H. Zhen; C. Cheung; C. Leung; Y. Choy, International Journal of Hydrogen Energy 37 (7) (2012) 6097-6105
[9] H. Zhen; C. Cheung; C. Leung; Y. Choy, International Journal of Hydrogen Energy 37 (14) (2012) 10947-10955.
[10] L. Dong; C. Cheung; C. Leung, International Journal of Heat and Mass Transfer 50 (25) (2007) 5124-5138
[11] L. Dong; C. Cheung; C. Leung, International journal of heat and mass transfer 50 (25) (2007) 5108-5123
[12] L. Dong; C. Cheung; C. Leung, Energy 49 (2013) 182-192
[13] E. Fernandes; R. Leandro, Combustion and flame 146 (4) (2006) 674-686
[14] T. Foat; K. Yap; Y. Zhang, Combustion and flame 125 (1) (2001) 839-851 .
[15] I. Boxx; C. Heeger; R. Gordon; B. Böhm; M. Aigner; A. Dreizler; W. Meier, Proceedings of the Combustion Institute 32 (1) (2009) 905-912

[16] J. Yu; V. Vuorinen; H. Hillamo; T. Sarjovaara; O. Kaario; M. Larmi, Journal of Natural Gas Science and Engineering 9 (2012) 1-10
[17] S. Specchia; G. Toniato, Catalysis Today 147 (2009) S99-S106.
[18] S.-S. Hou; Y.-C. Ko, Energy conversion and management 45 (9) (2004) 1583-1595
[19] S. Chander; A. Ray, Energy conversion and Management 46 (18) (2005) 2803-2837.
[20] L. Dong; C. Leung; C. Cheung, International journal of heat and mass transfer 46 (1) (2003) 113-125.
[21] W.-D. Hsieh; T.-H. Lin, Energy conversion and management 46 (5) (2005) 727-739.
[22] L. Kwok; C. Leung; C. Cheung, International journal of heat and mass transfer 48 (9) (2005) 1727-1738
[23] A. Milson; N. Chigier, Combustion and Flame 21 (3) (1973) 295-305
[24] M. Remie; M. Cremers; K. Schreel; L. de Goey, International journal of heat and mass transfer 50 (13) (2007) 2816-2827 .
[25] M. Remie; G. Särner; M. Cremers; A. Omrane; K. Schreel; L. Aldén; L. De Goey, International Journal of Heat and Mass Transfer 51 (11) (2008) 3144-3152
[26] R. Viskanta, Experimental Thermal and Fluid Science 6 (2) (1993) 111-134
[27] H. W. Huang; J. Yang; Q. Wang; Y. Zhang, Fuel 103 (2013) 334-346
[28] H. W. Huang; Y. Zhang, International Journal of Hydrogen Energy 37 (6) (2012) 5257-5267
[29] J. Fu; C. Tang; W. Jin; L. D. Thi; Z. Huang; Y. Zhang, international journal of hydrogen energy 38 (3) (2013) 1636-1643
[30] E. Mastorakos, Progress in Energy and Combustion Science 35 (1) (2009) 57-97
[31] Y. Zhang; K. Bray, Combustion and flame 116 (4) (1999) 671-674